Progress of Theoretical Physics, Vol. 46, No. 1, July 1971

Superfluid State in Neutron Star Matter. II

——*Properties of Anisotropic Energy Gap of* $^3P_2$ *Pairing*——

Tatsuyuki TAKATSUKA and Ryozo TAMAGAKI*

Department of Nuclear Engineering, Kyoto University, Kyoto
**Research Institute for Fundamental Physics, Kyoto University, Kyoto*

(Received January 22, 1971)

By applying the formulation developed in I and using several semiphenomenological two-nucleon potentials, properties of the $^3P_2$ pairing originating from spin-orbit forces are investigated at high density ($\rho \gtrsim 2\times10^{14}$gcm^{-3}) in neutron star matter. All the possible types of solutions are obtained by solving a coupled integral gap equation through an iterative procedure. Two of these five solutions represent axially symmetric energy gap. By a kind of self-consistency implied in the coupled gap equation the most general solution shows remarkable deviation from axial symmetry as a result of the mixing mainly of $m_j=\pm2, 0$ components but the resulting gap is nodeless. The total energy shifts are very close for all the types of solutions. Although calculations show the largest energy shift for the most general solution, this conclusion is a delicate quantitative one. The $^3P_2$ gap at high densities depends critically on the effective mass and short-range behavior of nuclear forces, especially on the strong repulsive core of two-nucleon forces. In any case there exists neutron superfluidity due to the $^3P_2$ pairing at least in the density region $\rho \cong (2\sim5)\times10^{14}$gcm^{-3}. Consequences of the calculated results are discussed, and an argument is given to the connection between the mass of the pulsar and the strong density dependence of neutron superfluidity.

§ 1. Introduction

Realization of superfluidity of the $^3P_2$ type in neutron star matter has been pointed out in previous paper I.[1] In connection with this suggestion the following points should be remarked:

(1) Superfluidity of neutrons exists owing to the $^3P_2$ pairing even in the high density region of neutron stars ($\rho \gtrsim 2\times10^{14}$g cm^{-3}) where the superfluidity due to the usual $^1S_0$ pairing disappears. This is a reliable theoretical consequence that nonzero angular momentum pairing does indeed take place.

(2) Recently, Baym, Pethick, Pines and Ruderman have pointed out an evidence for the superfluidity of both neutrons and protons in the interior of the pulsar on the basis of the slow relaxation after the discontinuous speed up of the rotation of the Vela pulsar which is considered to occur as a result of "starquake".[2] Unless mass of a neutron star is much smaller than $M_\odot$, a large portion of neutrons are in the $^3P_2$ superfluid state, while protons are in the $^1S_0$ superfluid state.

(3) The $^3P_2$ pairing originates from strong spin-orbit forces mainly due to the vector meson exchange in the intermediate and innermost regions, $r \cong 1\sim2$

fm and $r \lesssim 1$ fm respectively, r being the internucleon distances.[3] Nuclear forces in the innermost region are closely related to the upper limit of the density, beyond which the $^3P_2$ superfluidity disappears.

(4) Properties of neutron stars (thermal, rotational, magnetic and so on) are considerably affected by those of the neutron matter in the $^3P_2$ superfluid phase. It is also interesting to see how the shape of the Fermi surface deforms due to the anisotropy of the $^3P_2$ gap and which direction of the deformation is preferable with respect to the rotation axis.

From the viewpoint of many-body theory of neutron stars it is important to determine basic properties of the $^3P_2$ energy gap. Formulation to treat the non-zero angular momentum pairing has been developed in I. The gap equation is a coupled integral equation for five independent components, and is not easy to solve. Thus far, only simple special solutions have been dealt with. In I we have calculated the maximum $|m_J|$ coupling case, where only $m_J = \pm 2$ components are included. Another type of special solutions ($m_J = 0$ only)[1] has been discussed by Hoffberg, Glassgold, Richardson and Ruderman.[4] Angle dependence of the energy gap changes depending on what components in the gap matrix defined by Eq. (9) play an important role. There may be nodes of the energy gap in some directions. For example, the $^3P_2$ gap vanishes at $\theta = 0$ and π for the maximum $|m_J|$ coupling. The existence of nodes of the energy gap has much influence on properties of matter such as specific heat[5] and moment of inertia.[6] It is one of the aims of this paper to find the most general solution and the angle dependence of the energy gap, with ellucidating physical meaning of special solutions.

Previous calculations were performed by making use of phenomenological nonlocal separable potentials which simplify calculations. It is another aim of this paper to obtain more reliable conclusions by using semiphenomenological two-nucleon forces. In particular we pay attention to the effect of repulsive core. For the potentials with singular repulsive core, the usual way to calculate the energy gap (two-step method) is to get the reaction matrix at the Fermi surface and next to solve the gap equation neglecting the momentum dependence of the reaction matrix elements in a narrow region near E_F.[5),7] It is inevitable to introduce a parameter, an interval of integration, in the last step. On the other hand, it has been conjectured by Cooper, Mills and Sessler[8] and rigorously shown by Marumori, Murota, Takagi, Tanaka and Yasuno[9] that the gap equation is not altered even in the presence of a singular potential because the quantity such as $\Delta(k)/\sqrt{\tilde{\varepsilon}_k^2 + \Delta^2(k)}$ has dual roles not only to include the pairing correlation near E_F but also to imply the short-range correlation far from E_F. Therefore, if we employ a soft core potential, we can perform calculations unambiguously. The $^1S_0$ pairing in nuclear matter was successfully treated by this procedure by Ishihara, Tanaka, Yasuno and one of the authors (R.T.).[10] We adopt this procedure (one-step method) in this paper.

As in I, a small effect of the $^3F_2$ coupling due to tensor force is neglected.

Because this effect is attractive, the conclusions obtained here are not weakened by including this tensor coupling effect, except for the case of the critical situation where the gap becomes vanishingly small.

In § 2, we recapitulate the formula in I which we need for calculations of the $^3P_2$ gap equation. Two-nucleon potentials employed in calculations are explained in § 3. In § 4 we investigate two simple solutions with axial symmetry which are important to choose starting values for more general solutions. Also dependences on potential properties and effective mass are investigated. Mixing of different components in the gap matrix and departure from axial symmetry as a result of this mixing are obtained by looking for more general solutions in § 5. Section 6 is devoted to discussions of calculated results. In § 7 main conclusions are summarized and an argument is given concerning the mass of the Vela pulsar.

§ 2. Gap equation for $^3P_2$ pairing

In this section, we briefly summarize the treatment of the pairing interaction with nonzero angular momentum in I. If the attractive interaction is dominant in a particular pair state $\lambda(l, s, j)$, superfluidity is mainly determined by this λ-state pair interaction and the remaining parts of the interaction are to be treated in terms of quasiparticle operators after a generalized Bogoliubov transformation corresponding to the λ-pair interaction. As far as we are concerned with calculations of the energy gap and of the energy shift of the ground state due to the λ-pairing, we can simplify the problem in such a way that the system under consideration is described with a model Hamiltonian with the λ-pair interaction only:

$$H_\lambda \equiv H_0 + H_{\rm pair}^{(\lambda)}$$
$$= \sum_{k\sigma} \tilde{\varepsilon}_k C_{k\sigma}^* C_{k\sigma} + \sum_k \sum_{k'} \frac{(4\pi)^2}{\Omega} \langle k' | V_\lambda | k \rangle \sum_{mj} b_{\lambda mj}^*(k') b_{\lambda mj}(k), \tag{1}$$

where

$$\tilde{\varepsilon}_k = \hbar^2 (k^2 - k_F^2)/2M^*, \tag{2}$$

and

$$b_{\lambda mj}^*(k) = \frac{1}{\sqrt{2}} \sum_{\sigma_1} \sum_{\sigma_2} (1/2\ 1/2 \sigma_1 \sigma_2 | s m_s)\ (s l m_s m_l | j m_j) \int d\hat{k} Y_{lm_l}(\hat{k}) C_{k\sigma_1}^* C_{-k\sigma_2}^* \tag{3}$$

is a boson operator representing a λ-pair. For simplicity, we take into account the effect of one-body potential by introducing the effective mass M^* into $\tilde{\varepsilon}_{k'}$, the kinetic energy measured from the Fermi energy. Hereafter k and $\hat{k}$ denote the magnitude and the direction of the nucleon wave number vector $\boldsymbol{k}$, respectively.

The transformation of the Fermi gas state $|\Phi_0\rangle$ into the super state $|\Psi_0\rangle$ is given by the following generalized Bogoliubov transformation:

$$|\Psi_0\rangle = e^{iS}|\Phi_0\rangle\,, \tag{4}$$

$$S = -i\sum_{kmj}\{\phi_{\lambda mj}(k)\,b^*_{\lambda mj}(k) - \phi^*_{\lambda mj}(k)\,b_{\lambda mj}(k)\}\,. \tag{5}$$

Quasiparticle operators $\alpha_{k\rho}$ $(\rho=1,2)$ are obtained by the transformation

$$\boldsymbol{\alpha}_k = e^{iS}\boldsymbol{C}_k e^{-iS}, \qquad \boldsymbol{\alpha}_k{}^* = e^{iS}\boldsymbol{C}_k{}^* e^{-iS}, \tag{6}$$

where

$$\boldsymbol{C}_k \equiv \begin{pmatrix} C_{k\uparrow} \\ C_{k\downarrow} \end{pmatrix} \qquad \text{and} \qquad \boldsymbol{\alpha}_k \equiv \begin{pmatrix} \alpha_{k1} \\ \alpha_{k2} \end{pmatrix}.$$

By use of Eq. (6), the model Hamiltonian H_λ is rewritten in terms of quasiparticle operators:

$$H_\lambda \cong H_{00}(\text{constant terms}) + H_{11}(\alpha,\ \alpha^*\ \text{terms}) + H_{20}(\alpha^*\alpha^*,\ \alpha\alpha\ \text{terms}). \tag{7}$$

Elimination of the dangerous terms H_{20} leads to a gap equation, and the energy gap $D_\lambda(\boldsymbol{k})$ is given by the (2×2) gap matrix $\boldsymbol{\Delta}_\lambda(\boldsymbol{k})$ in spin space in the following way:

$$D_\lambda{}^2(\boldsymbol{k}) = \tfrac{1}{2}\,\mathrm{Tr}[\boldsymbol{\Delta}_\lambda(\boldsymbol{k})\,\boldsymbol{\Delta}_\lambda{}^\dagger(\boldsymbol{k})], \tag{8}$$

where

$$\boldsymbol{\Delta}_\lambda(\boldsymbol{k}) = \sum_{m_j=-j}^{j}\Delta_{\lambda m_j}(k)\,G_{\lambda m_j}(\hat{k}), \tag{9}$$

$$[G_{\lambda m_j}(\hat{k})]_{\sigma_1,\sigma_2} = (1/2\ 1/2\sigma_1\sigma_2|sm_s)\ (slm_s m_j - m_s|jm_j)\ Y_{l,m_j-m_s}(\hat{k}), \tag{10}$$

and the total energy shift ΔE is given by the following relation:

$$\Delta E = H_{00} - 2\sum_{k(<k_F)}\tilde{\varepsilon}_k\,. \tag{11}$$

The quasiparticle kinetic energy H_{11} becomes

$$H_{11} = \sum_{\boldsymbol{k}}\sum_{\rho}\sqrt{\tilde{\varepsilon}_k{}^2 + D_\lambda{}^2(\boldsymbol{k})}\,\alpha^*_{k\rho}\alpha_{k\rho}\,. \tag{12}$$

Here, we write down explicitly the gap equation for $\Delta_{\lambda m_j}(k)$ in the case of ${}^3P_2$ pairing $(\lambda;\ s=1,\ l=1,\ j=2)$:

$$\begin{cases} \Delta_{\lambda m_j}(k) = -\dfrac{1}{\pi}\displaystyle\int dk'k'^2\langle k'|V_\lambda|k\rangle\int d\hat{k}'\,\frac{\sum_\mu \Delta_{\lambda\mu}(k')\,\mathrm{Tr}[G_{\lambda\mu}(\hat{k}')\,G^*_{\lambda m_j}(\hat{k}')]}{\sqrt{\tilde{\varepsilon}^2_{k'} + D_\lambda{}^2(\boldsymbol{k}')}}\,, \\ D_\lambda{}^2(\boldsymbol{k}) = \tfrac{1}{2}\displaystyle\sum_{m_j}\sum_{\mu}\Delta_{\lambda m_j}(k)\,\Delta^*_{\lambda\mu}(k)\,\mathrm{Tr}[G_{\lambda m_j}(\hat{k})\,G^*_{\lambda\mu}(\hat{k})], \\ [G_{\lambda m_j}(\hat{k})]_{\sigma_1,\sigma_2} \equiv (1/2\ 1/2\sigma_1\sigma_2|1m_s)\ (11m_s m_j - m_s|2m_j)\ Y_{1,m_j-m_s}(\hat{k})\,. \end{cases} \tag{13}$$

The condition that the transformation (5) is invariant under time reversal leads to the relation $\phi^*_{\lambda m_j}(k) = (-)^{j+m_j}\phi_{\lambda -m_j}(k)$, from which we get

$$\Delta^*_{\lambda m_j}(k) = (-)^{j+m_j}\Delta_{\lambda -m_j}(k)\,. \tag{14}$$

Then, $\Delta_{\lambda m_j}(k)$ is expressed by only five independent variables as follows:

$$\begin{cases} \Delta_2(k) \equiv \delta_2(k) + i\eta_2(k), \\ \Delta_1(k) \equiv \delta_1(k) + i\eta_1(k), \\ \Delta_0(k) \equiv \delta_0(k), \end{cases} \tag{15}$$

where $\delta_2(k)$, $\eta_2(k)$, $\delta_1(k)$, $\eta_1(k)$ and $\delta_0(k)$ are real. Substituting Eq. (15) into Eq. (13) we obtain the following nonlinear coupled integral equations:

$$\begin{aligned} \delta_2(k) = &-\frac{1}{\pi}\int dk' k'^2 \langle k'|V_\lambda|k\rangle \int d\hat{k}' \\ &\times \frac{3}{8\pi}\Big[\delta_2(k')\sin^2\theta - \delta_1(k')\sin\theta\cos\theta\cos\phi - \eta_1(k')\sin\theta\cos\theta\sin\phi \\ &-\frac{1}{\sqrt{6}}\delta_0(k')\sin^2\theta\cos 2\phi\Big]\Big/\sqrt{\tilde{\varepsilon}_{k'}^2 + D_\lambda^2(\boldsymbol{k}')}, \end{aligned} \tag{16·1}$$

$$\begin{aligned} \eta_2(k) = &-\frac{1}{\pi}\int dk' k'^2 \langle k'|V_\lambda|k\rangle \int d\hat{k}' \\ &\times \frac{3}{8\pi}\Big[\eta_2(k')\sin^2\theta - \eta_1(k')\sin\theta\cos\theta\cos\phi + \delta_1(k')\sin\theta\cos\theta\sin\phi \\ &+\frac{1}{\sqrt{6}}\delta_0(k')\sin^2\theta\sin 2\phi\Big]\Big/\sqrt{\tilde{\varepsilon}_{k'}^2 + D_\lambda^2(\boldsymbol{k}')}, \end{aligned} \tag{16·2}$$

$$\begin{aligned} \delta_1(k) = &-\frac{1}{\pi}\int dk' k'^2 \langle k'|V_\lambda|k\rangle \int d\hat{k}' \\ &\times \frac{3}{8\pi}\Big[-\delta_2(k')\sin\theta\cos\theta\cos\phi + \eta_2(k')\sin\theta\cos\theta\sin\phi \\ &+\delta_1(k')\left(1-\frac{1}{2}\sin^2\theta\right) + \frac{1}{2}\delta_1(k')\sin^2\theta\cos 2\phi - \frac{1}{2}\eta_1(k')\sin^2\theta\sin 2\phi \\ &-\frac{1}{\sqrt{6}}\delta_0(k')\sin\theta\cos\theta\cos\phi\Big]\Big/\sqrt{\tilde{\varepsilon}_{k'}^2 + D_\lambda^2(\boldsymbol{k}')}, \end{aligned} \tag{16·3}$$

$$\begin{aligned} \eta_1(k) = &-\frac{1}{\pi}\int dk' k'^2 \langle k'|V_\lambda|k\rangle \int d\hat{k}' \\ &\times \frac{3}{8\pi}\Big[-\eta_2(k')\sin\theta\cos\theta\cos\phi - \delta_2(k')\sin\theta\cos\theta\sin\phi \\ &+\eta_1(k')\left(1-\frac{1}{2}\sin^2\theta\right) - \frac{1}{2}\eta_1(k')\sin^2\theta\cos 2\phi - \frac{1}{2}\delta_1(k')\sin^2\theta\sin 2\phi \\ &+\frac{1}{\sqrt{6}}\delta_0(k')\sin\theta\cos\theta\sin\phi\Big]\Big/\sqrt{\tilde{\varepsilon}_{k'}^2 + D_\lambda^2(\boldsymbol{k}')}, \end{aligned} \tag{16·4}$$

$$\delta_0(k) = -\frac{1}{\pi}\int dk' k'^2 \langle k'|V_\lambda|k\rangle \int d\hat{k}'$$

$$\times\frac{3}{8\pi}\Big[-\frac{2}{\sqrt{6}}\delta_2(k')\sin^2\theta\cos 2\phi+\frac{2}{\sqrt{6}}\eta_2(k')\sin^2\theta\sin 2\phi$$
$$-\frac{2}{\sqrt{6}}\delta_1(k')\sin\theta\cos\theta\cos\phi+\frac{2}{\sqrt{6}}\eta_1(k')\sin\theta\cos\theta\sin\phi$$
$$+\delta_0(k')\left(\frac{1}{3}+\cos^2\theta\right)\Big]\Big/\sqrt{\tilde{\varepsilon}_{k'}^2+D_\lambda^2(\boldsymbol{k}')}, \tag{16·5}$$

where

$$D_\lambda^2(\boldsymbol{k}')=\frac{1}{8\pi}\Big[3(\delta_2^2(k')+\eta_2^2(k'))\sin^2\theta+3(\delta_1^2(k')+\eta_1^2(k'))\left(1-\frac{1}{2}\sin^2\theta\right)$$
$$+\frac{1}{2}\delta_0^2(k')(1+3\cos^2\theta)$$
$$+\sqrt{6}(\delta_0(k')\eta_1(k')+\sqrt{6}\delta_1(k')\eta_2(k')-\sqrt{6}\eta_1(k')\delta_2(k'))\sin\theta\cos\theta\sin\phi$$
$$-\sqrt{6}(\delta_0(k')\delta_1(k')+\sqrt{6}\delta_1(k')\delta_2(k')+\sqrt{6}\eta_1(k')\eta_2(k'))\sin\theta\cos\theta\cos\phi$$
$$+\frac{1}{2}(3\delta_1^2(k')-3\eta_1^2(k')-2\sqrt{6}\delta_0(k')\delta_2(k'))\sin^2\theta\cos 2\phi$$
$$+\frac{1}{2}(2\sqrt{6}\delta_0(k')\eta_2(k')-6\delta_1(k')\eta_1(k'))\sin^2\theta\sin 2\phi\Big]. \tag{17}$$

The coupled equations (16) combined with Eq. (17) are not easy to solve. But if we find suitable starting values, we can solve these equations numerically by the iterative method. Therefore, the first step in computation is to find a set of starting values so as to converge iterations. In order to find such a set we begin with particular cases in which physical meaning is clear, and then treat more general cases. That is, we start with solving the gap equations for the maximum $|m_j|$ coupling (only $m_j=\pm 2$ components are used) and the $m_j=0$ coupling.

§ 3. Potentials for $^3P_2$ state

In this section, we explain the potentials used in our calculations of the $^3P_2$ energy gap.

(1) *Nonlocal separable potential*

This potential is one of nonlocal separable potentials without repulsive core adjusted to nucleon-nucleon scattering phase shifts up to $E_{N-N}^{(\mathrm{Lab})}<400$ MeV by Mongan:[11]

$$\langle k'|V_\lambda|k\rangle=-\frac{\pi}{2}h_l(k')h_l(k),$$
$$h_l(k)=C_A k^l/(k^2+a_A^2)^{(l+n)/2}$$

with $l=1$, $n=1$, $C_A=5.349\,(\mathrm{MeV\cdot fm})^{1/2}$, $a_A=1.509\,\mathrm{fm}^{-1}$. This potential is adopted in order to compare our results in this paper with those in I for $|m_j|=2$ by use of the dispersion relation, and also those of Ref. 4) for $m_j=0$ calculated with Tabakin's nonlocal separable potential which is essentially the same as Mongan's. The results by use of this potential shown later are consistent with those of the previous works.

(2) *OPEG*

Local potentials referred to as OPEG (Gaussian soft core potential with the OPEP tail) is the most reliable among potentials used here. Its inside properties have been determined semiphenomenologically. The $^3P_2$ effective potential is

$$V_\lambda(r)=V_C(r)-0.4V_T(r)+V_{LS}(r)+\tfrac{1}{3}V_W(r)+2V_{LL}(r).$$

$V_C(r)$ has Gaussian repulsive core and $V_{LS}(r)$ is strongly attractive for $r\lesssim 1$ fm. Two potentials of this type are employed in calculations. The one is OPEG $^3O-1$ in Table II of Ref. 12)*) with 2 GeV repulsive core and a steep $V_{LS}(r)$ with -1500 MeV at $r=0$, which partially cancel each other in the $^3P_2$ state and give 500 MeV core to $V_\lambda(r)$ as shown in Fig. 1. The other is a slightly modified version of OPEG $^3O-2$ in Ref. 12) with 300 MeV core and a softened spin-orbit potential ($V_{LS}(r=0)=-100$ MeV). Modification is done only in $V_{LS}(r)$ by changing the depth of the Gaussian term, to improve the $^3P_2$ fit slightly: from $\mathcal{C}V^0_{LS}=-100$ MeV (original in Table II of Ref. 12) to $\mathcal{C}V^0_{LS}=-150$ MeV (modified). We denote this as OPEG $^3O-2$M, which is almost the same as OPEG $^3O-1$ for $r\gtrsim 0.8$ fm and has a somewhat shrinked core with 150 MeV in $V_\lambda(r)$

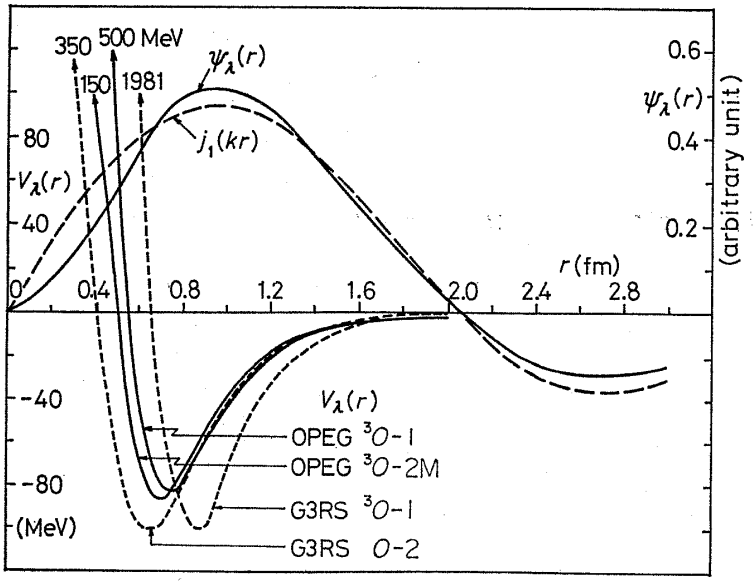

Fig. 1. Local effective potentials $V_\lambda(r)$ for OPEG and G3RS types in the $^3P_2$ state. The values attached to the arrows are $V_\lambda=V_C+V_{LS}$ at $r=0$. $\psi_\lambda(r)$ is the correlated $^3P_2$-pair radial wave function calculated from G3RS $^3O-1$ for $m^*=1$ and $E_F=100$ MeV. The corresponding uncorrelated function $j_1(k_Fr)$ normalized to $\psi_\lambda(r)$ at $r=1.4$ fm is also shown for comparison.

*) The abbreviations, ^3O and ^1E, stand for the triplet odd and singlet even states of the two-nucleon system, respectively.

as shown in Fig. 1. The calculated $^3P_2$ phase shifts are shown in Fig. 2.

(3) *G3RS*

Local potentials referred to as G3RS (Gaussian soft core potential with three ranges) have the following form:

$$V_\lambda(r) = V_C(r) - 0.4V_T(r) + V_{LS}(r) + \tfrac{1}{3}V_W(r) + 2V_{LL}(r),$$

$$V_i(r) = \sum_{n=1}^{3} v_{in} \exp[-(r/\eta_{in})^2] \qquad \text{for } i = C,\ T,\ LS,\ W,\ LL.$$

In this case, 2.43 GeV core potential is denoted by G3RS $^3O-1$ and 350 MeV core potential by G3RS $^3O-2$ in Table III of Ref. 12). As shown in Fig. 1, $V_\lambda(r)$ of G3RS $^3O-1$ is more attractive outside a stronger repulsive core than that of OPEG $^3O-1$ and $V_\lambda(r)$ of G3RS $^3O-2$ has a more shrinked repulsive core than that of OPEG ^3O-2M. G3RS $^3O-1$ can be regarded as an extreme of OPEG $^3O-1$ type and G3RS $^3O-2$ as the other extreme of OPEG ^3O-2M type. The matrix elements of Gaussian potentials are easily calculated, and we can shorten the computing time by making use of this type. Calculation for general solutions is made by use of G3RS $^3O-1$. The calculated $^3P_2$ phase shifts are shown in Fig. 2.

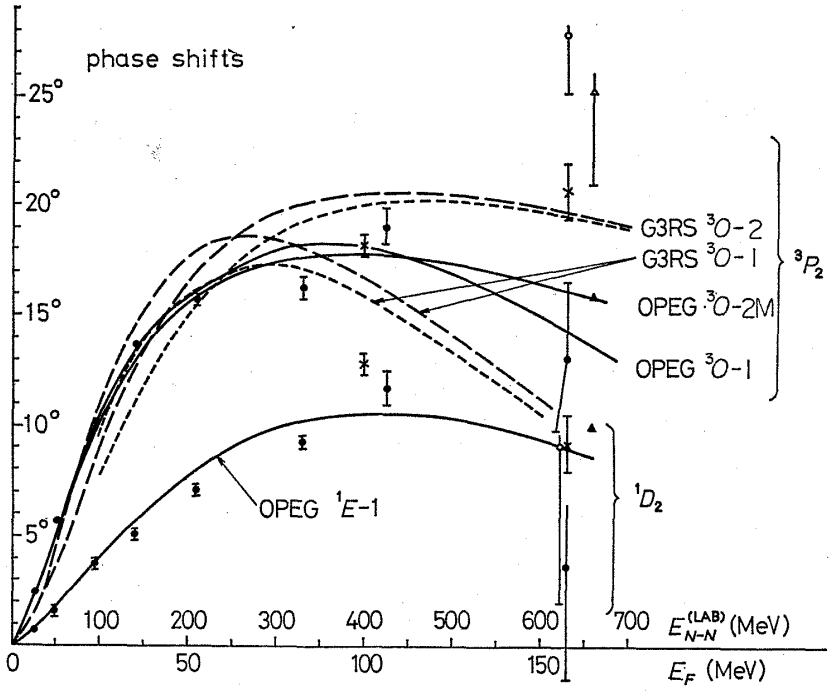

Fig. 2. $^3P_2$ scattering phase shifts calculated from OPEG (solid lines) and G3RS (dashed lines) with $^3F_2$ coupling and G3RS (dotted curves) without $^3F_2$ coupling. $^1D_2$ scattering phase shifts obtained from OPEG $^1E-1$[12] are shown for discussions in § 6-3. The indicated solutions of phase shift analysis follows the figure caption of Fig. 1 in I.

§ 4. Axially symmetric energy gap

Generally speaking, the $^3P_2$ gap equation is expressed by Eq. (16), where

all the m_j components ($m_j=2, 1, 0, -1, -2$) are coupled. As the first step, if we impose the condition that the existence of a gap deforms the Fermi sphere in an axially-symmetric way, the axial-symmetry of $D_\lambda^2(\boldsymbol{k})$ in Eq. (17) leads to the following relations, equivalent to Eq. (4) in Ref. 4) given by Hoffenberg et al.:

$$\begin{cases} \delta_0\eta_1+\sqrt{6}\delta_1\eta_2-\sqrt{6}\eta_1\delta_2=0\,, \\ \delta_0\delta_1+\sqrt{6}\delta_1\delta_2+\sqrt{6}\eta_1\eta_2=0\,, \\ 2\sqrt{6}\delta_0\eta_2-6\delta_1\eta_1=0\,, \\ 3\delta_1^2-3\eta_1^2-2\sqrt{6}\delta_0\delta_2=0\,. \end{cases} \tag{18}$$

From Eq. (16) together with Eq. (18), we get $\delta_2=\eta_2$, $\delta_1=\eta_1$, then the solutions satisfying this condition reduce to only two simple ones:

Sol. 1: the solution with only $m_j=2, -2$ components ($\delta_1=\eta_1=\delta_0=0$),

Sol. 2: the solution with only $m_j=0$ component ($\delta_2=\eta_2=\delta_1=\eta_1=0$).

These two simple solutions satisfy Eq. (16) self-consistently and exhaust all the solutions obtained under the condition of axial symmetry of the energy gap.

4-1 *Solution with maximum $|m_j|$ coupling and potential dependence of $^3P_2$ energy gap*

This solution (Sol. 1) corresponds to the case in which only the pair states with the complete alignment of the spin and angular momenta are selected. The energy gap $D_\lambda(\boldsymbol{k})=\sqrt{3/8\pi}\,\Delta_2(k)\sin\theta$ vanishes at $\theta=0$ and π, and the deformation of the Fermi sphere is axially symmetric and oblate. Putting $\delta_1=\eta_1=\delta_0=0$ and $\delta_2=\eta_2=\Delta_2/\sqrt{2}$ in Eq. (16), we have

$$\Delta_2(k)=-\frac{1}{\pi}\int dk'k'^2\langle k'|V_\lambda|k\rangle\int d\hat{k}'\frac{(3/8\pi)\Delta_2(k')\sin^2\theta}{\sqrt{\tilde{\varepsilon}_{k'}^2+(3/8\pi)\Delta_2^2(k')\sin^2\theta}}\,. \tag{19}$$

The resulting energy gaps $\Delta_2(k)$ calculated from various potentials are shown in Fig. 3 for the effective mass parameter $m^*\equiv M^*/M=1$ and $E_F=100$ MeV. In the region of large k where the short range correlation plays an important role, $\Delta_2(k)$ becomes negative due to the effect of repulsive core, because

$$\Delta_2(k)/\tilde{E}(k)\equiv\int d\hat{k}\,(3/8\pi)\sin^2\theta\Delta_2(k)/\sqrt{\tilde{\varepsilon}_k^2+(3/8\pi)\Delta_2^2(k)\sin^2\theta}$$

means the pair correlation function of both the BCS type and the short-range repulsion. In Fig. 1 a correlated pair wave function

$$\psi_\lambda(r)=\int_0^\infty dkk^2j_1(kr)\Delta_2(k)/\tilde{E}(k)$$

for $E_F=100$ MeV and $m^*=1$ is shown so as to illustrate such a situation. Short-range correlation is not very strong except for G3RS $^3O-1$.

The resulting energy gaps $\Delta_2(k_F)$ at the Fermi surface for various cases are given in Table I, which shows the existence of the $^3P_2$ gap larger than about 1 MeV in so far as the $^3P_2$ potentials reproduce well the $^3P_2$ phase shifts below

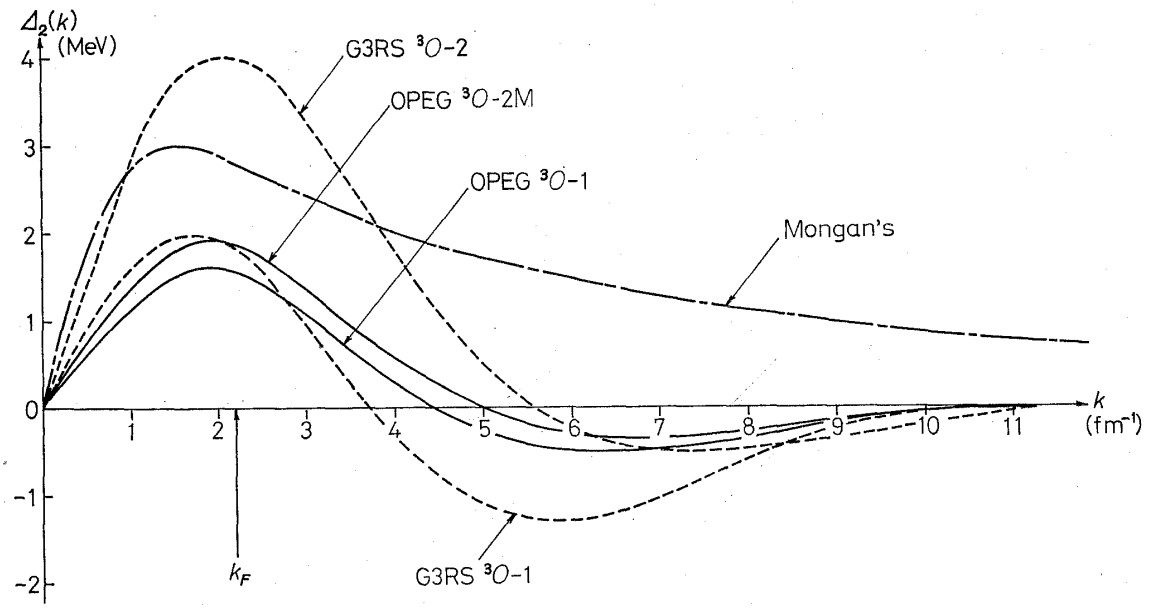

Fig. 3. Energy gap function $\Delta_2(k)$ calculated from various potentials for the effective mass parameter $m^*=1$ and the Fermi energy $E_F=100$ MeV.

Table I. Values of the energy gap in MeV at $k=k_F$ in the case of Sol. 1 ($m_j=\pm 2$) and Sol. 2 ($m_j=0$) calculated from various potentials for typical values of E_F and m^*.

m_j	E_F	m^*	OPEG $^3O-1$	OPEG ^3O-2M	G3RS $^3O-1$	G3RS $^3O-2$	MONGAN'S
± 2 (Sol. 1)	50	1	0.28	0.39	0.63	0.37	0.72
	75	1	1.04	1.12	1.65	1.95	1.84[a]
		0.8	0.02	0.01	0.38	0.54	0.37[a]
	100	1	1.54	1.89	1.83	3.98	2.81
		0.9	0.89	1.14	1.05	2.51	1.42[a]
		0.8	0.11	0.39	0.27	1.43	0.66[a]
	125	1	1.65	2.34	1.32	5.61	3.44[a]
	150	1	1.47	2.41	0.79	6.50	3.95
	175	1	0.55	2.22	0.38	6.70	4.12[a]
	200	1	0.01	1.60	<0.01	6.31	4.26
0 (Sol. 2)	75	0.8	0.02	0.01	0.53	0.78	
	100	1	2.22	2.72	2.64	5.71	4.03

a) calculated by use of the dispersion relation in I.

$E_{N-N}^{(\mathrm{LAB})}<400$ MeV and the effective mass $M^*\simeq M$. The dependences of $\Delta_2(k_F)$ on various factors are summarized as follows:

(i) Dependence on potential properties

It is found that the magnitude of the energy gap $\Delta_2(k_F)$ depends sensitively on the properties of the matrix elements $\langle k|V_\lambda|k_F\rangle$ shown in Fig. 4. The magnitude of $\Delta_2(k_F)$ is mainly determined by the matrix elements $\langle k|V_\lambda|k_F\rangle$ neighbouring $k=k_F$ in so far as the tail of the matrix elements for $k\gtrsim 5$ fm has the

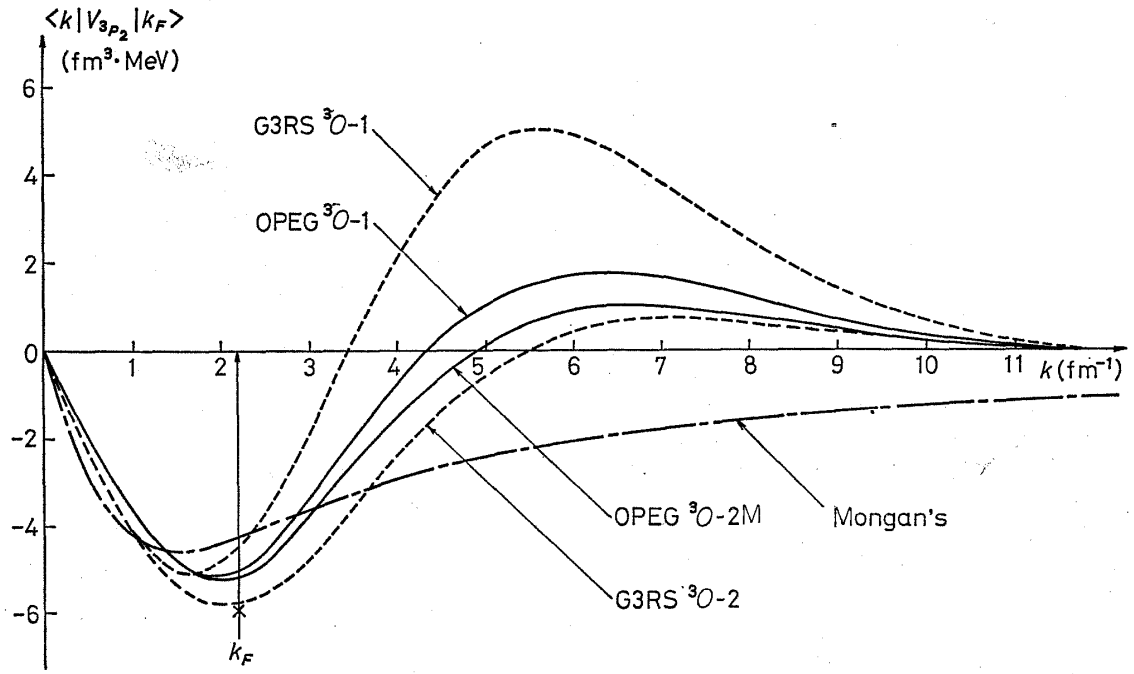

Fig. 4. k-dependence of the $^3P_2$ matrix element $\langle k|V_\lambda|k_F\rangle$ of various potentials for $E_F=100$ MeV. The cross on the $k=k_F$ line is the extrapolated value of $^3P_2$ reaction matrix element $\langle k_F|G|k_F\rangle$ for OPEG $^3O-1$ obtained by Ikeuchi et al.[13]

same qualitative feature. This aspect can be seen by comparing the matrix elements of OPEG $^3O-2$M with that of G3RS $^3O-2$ to produce a very large $\Delta_2(k_F)$. Also, the k-dependence of the matrix elements influences considerably the energy gap. For example, although the matrix element $\langle k_F|V_\lambda|k_F\rangle$ of G3RS $^3O-1$ is slightly more attractive than that of Mongan's potential, $\Delta_2(k_F)$ for the former is smaller than that for the latter. This is caused by the fact that the former has a strong repulsive tail for $k\gtrsim 3.5$ fm^{-1} and the latter has a long attractive tail, that is to say, by the different short-range correlation. This statement can be confirmed by comparing the OPEG $^3O-1$ and the OPEG $^3O-2$M cases.

(ii) Dependence on effective mass

The m^*-dependence of the energy gap $\Delta_2(k_F)$ is given in Table I for $E_F=75$ and 100 MeV and illustrated in Figs. 5(a) and 5(b) for $E_F=100$ MeV. The strong m^*-dependence shown there means that one should be careful in choosing the effective mass from the neutron single particle potential $V_n(k)$. In the den-

sity region, $\rho \cong 2 \sim 8 \times 10^{14}$g cm^{-3} ($E_F \cong 50 \sim 120$ MeV), m^* is estimated as 0.84, 0.81 and 0.71 corresponding to $\rho = 2.3$, 4.0 and 7.8×10^{14}g cm^{-3} from $V_n(k)$ obtained for OPEG potential in the work on the equation of state and models of neutron stars by Ikeuchi, Nagata, Mizutani and Nakazawa.[13]

To test the accuracy of the effective mass approximation in this density region, calculations of $\Delta_2(k)$ are made by use of the following $V_n(k)$ at $E_F = 75$ MeV:

$$V_n(k) = -50e^{-0.14k^2} - 17e^{-0.095k^2}, \qquad V_n \text{ in MeV and } k \text{ in fm}^{-1},$$

which is adjusted to the one obtained by Ikeuchi et al.[13] for $k < k_F$ and tends to zero as $k \to \infty$. $\Delta_2(k_F)$ thus calculated for G3RS $^3O-1$ is 0.44 MeV, which is slightly larger than $\Delta_2(k_F) = 0.38$ MeV by the effective mass approximation with $m^* = 0.8$. This means the adequateness of this approximation.

For $m^* \simeq 0.8$, the $^3P_2$ gap exists but becomes quite small: $\Delta_2(k_F) = 0.1 \sim 0.4$ MeV at $\rho = 2 \sim 5 \times 10^{14}$g cm^{-3} for potentials with repulsive core. However, if m^* becomes smaller than 0.7 at higher densities ($\rho \gtrsim 8 \times 10^{14}$g cm^{-3}; $E_F \gtrsim 120$ MeV) as inferred from Ref. 13), the $^3P_2$ gap disappears. If the effective potential in the $^3P_2$ state has no short-range repulsion, we have somewhat wider density region where the $^3P_2$ gap exists. Even in such a case, the reduction of m^* acts to diminish or vanish the $^3P_2$ gap, as indicated by Fig. 6 in I. Here we want to remark that the value of m^* at the high density ($\rho \gtrsim 6 \times 10^{14}$g cm^{-3}; $E_F > 100$ MeV) should not be taken too seriously, since the Brueckner theory adopted to get the single particle energy becomes less reliable at such high densities than at lower densities.

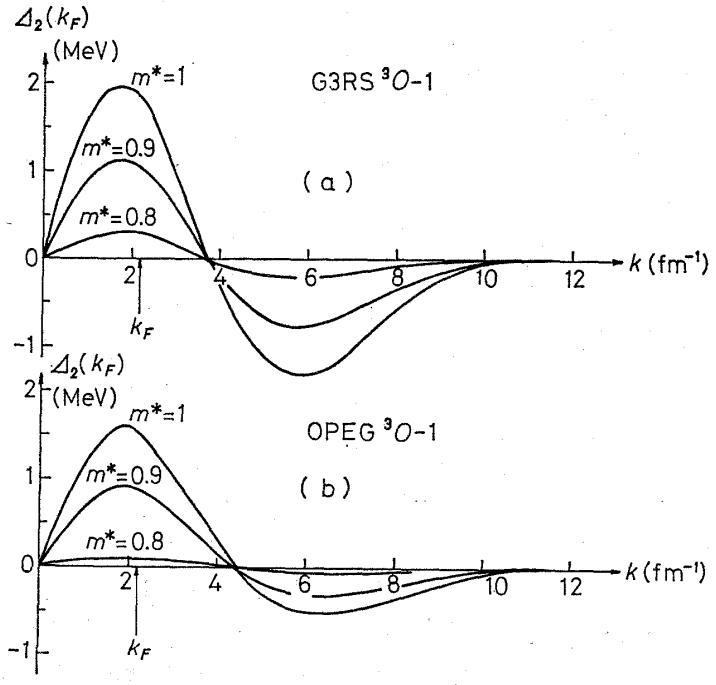

Fig. 5. Dependence of the energy gap $\Delta_2(k_F)$ on the effective mass parameter m^* for $E_F = 100$ MeV; Fig. 5(a) for G3RS $^3O-1$ potential and Fig. 5(b) for OPEG $^3O-1$ potential.

iii) Dependence on density

The ρ (or E_F) dependence of the gap $\Delta_2(k_F)$ is shown in Fig. 6 for $m^* = 1$ and 0.8. At low densities $E_F \lesssim 30$ MeV ($\rho \lesssim 1 \times 10^{14}$g cm^{-3}) the $^1S_0$ gap exists. Just above the density where this gap disappears, the $^3P_2$ gap begins to appear ($E_F \gtrsim 50$ MeV; $\rho \gtrsim 2 \times 10^{14}$g cm^{-3}).

The $^3P_2$ gap at high densities ($\rho \gtrsim 10^{15}$g cm^{-3}; $E_F \gtrsim 150$ MeV) critically depends on short-range be-

havior of the $^3P_2$ interaction. When the strong repulsive core is present, the $^3P_2$ gap disappears for $\rho \gtrsim 1.5 \times 10^{15}$g cm^{-3}, as in the case of G3RS $^3O-1$, even for $m^*=1$. On the other hand, if the attractive force is present even at short distances (for high k values), the $^3P_2$ gap grows very prominently, as for G3RS $^3O-2$ and Mongan's potential. The behaviors mentioned above survive also for smaller values of m^*, but the region of existence of the $^3P_2$ superfluidity shrinks to a narrower domain. Ikeuchi et al. obtained the $^3P_2$ gap, $\Delta_2(k_F) \sim 0.5$ MeV at $\rho=2.3 \times 10^{14}$g cm^{-3} by use of OPEG potential (OPEG $^3O-1$ in the triplet odd state) and the two-step method mentioned in § 1.[13] This $\Delta_2(k_F)$ larger than our corresponding value seems to be attributed to a different treatment of short-range correlation in solving the gap equation, since their $^3P_2$ reaction matrix element $\langle k_F|G|k_F\rangle$ for OPEG $^3O-1$ is close to $\langle k_F|V_\lambda|k_F\rangle$ for G3RS $^3O-2$, as indicated by the cross in Fig. 4.

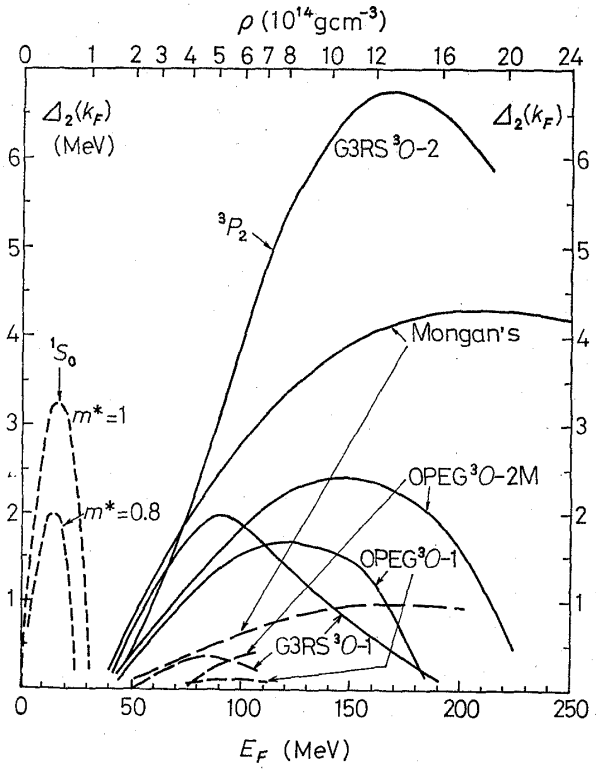

Fig. 6. Density dependence of the energy gap $\Delta_2(k_F)$ of Sol. 1 for $m^*=1$ and various potentials (solid lines). Several points of $\Delta_2(k_F)$ for $m^*=0.8$ are indicated (dashed lines). The $^1S_0$ energy gap is also shown by the dotted lines for comparison.

4-2 *Solution with only $m_j=0$ component*

This solution (Sol. 2) corresponds to the case in which only the pair state with $m_j=0$ is selected. The energy gap reaches the maximum value at $\theta=0$ and the deformation of the Fermi sphere is axially symmetric and prolate. Putting $\delta_0=\Delta_0$ and $\delta_2=\eta_2=\delta_1=\eta_1=0$ in Eq. (16), we have

$$\Delta_0(k) = -\frac{1}{\pi}\int dk' k'^2 \langle k'|V_\lambda|k\rangle \int d\hat{k}' \frac{\Delta_0(k')\,(1+3\cos^2\theta)/8\pi}{\sqrt{\tilde{\varepsilon}_{k'}^2+\Delta_0^2(k')\,(1+3\cos^2\theta)/16\pi}}. \qquad (20)$$

The k-dependence of the energy gap $\Delta_0(k)$ calculated from G3RS $^3O-1$ for $E_F=100$ MeV and $m^*=1$ is shown in Fig. 7, in comparison with that of $\Delta_2(k)$.

In Table I, we can see how the values of the energy gap $\Delta_0(k_F)$ for $E_F=100$ MeV and $m^*=1$ and for $E_F=75$ MeV and $m^*=0.8$ depend on potential properties. From this, we find the relation $\Delta_0(k_F) \simeq 1.44\Delta_2(k_F)$ irrespective of potentials. This relation is understood in the following way: If we neglect the

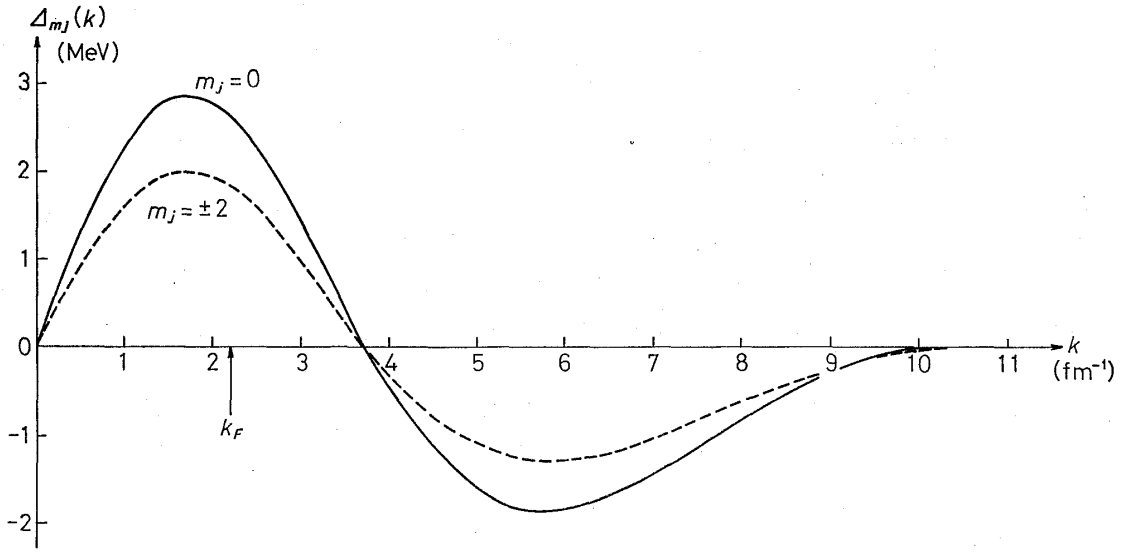

Fig. 7. The k-dependence of energy gap $\Delta_0(k)$ ($m_j=0$) of Sol. 2 calculated from G3RS $^3O-1$ for $E_F=100$ MeV and $m^*=1$. The energy gap $\Delta_2(k)$ ($m_j=\pm 2$) of Sol. 1 calculated from G3RS $^3O-1$ for $E_F=100$ MeV and $m^*=1$ is also shown for comparison.

angular dependence of the energy gap in Eqs. (19) and (20), the gap equation is written as

$$\Delta_2(k)=\int dk' f(k',k)\frac{\Delta_2(k')}{\sqrt{\tilde{\varepsilon}_{k'}^2+\Delta_2^2(k')}} \qquad \text{for Sol. 1}$$

and

$$\Delta_0(k)=\int dk' f(k',k)\frac{\Delta_0(k')}{\sqrt{\tilde{\varepsilon}_{k'}^2+\Delta_0^2(k')/2}} \qquad \text{for Sol. 2,}$$

where $f(k',k)$ is a function of k and k'. These equations result in the relation $\Delta_0(k)=\sqrt{2}\Delta_2(k)$ and this is the reason why the above-mentioned results occur. The shift from $\Delta_0(k_F)/\Delta_2(k_F)=\sqrt{2}$ is caused by the contribution from the angular dependence of the energy gap.

The m^*-dependence and $\rho(E_F)$-dependence of the energy gap $\Delta_0(k)$ are qualitatively similar to those of $\Delta_2(k)$ shown in Figs. 5 and 6, respectively, except for the absolute values that $\Delta_0(k)$ is about $\sqrt{2}$ times larger than $\Delta_2(k)$.

§ 5. Axially asymmetric energy gap

In this section, we generally treat the coupled equation (16) without the condition that the deformation of the Fermi sphere is axially symmetric. In this case, the energy gap matrix $\boldsymbol{\Delta}_\lambda(k)$ contains various m_j-components and $D_\lambda^2(\boldsymbol{k})$ has the ϕ-dependence as well as the θ-dependence.

Taking the self-consistency of the gap equation (16) into account, we find that the solutions of this equation are confined to the following three cases:

Sol. 3: the solution where $m_j=0,\ 2,\ -2$ components are coupled ($\delta_1=\eta_1=0$).

Sol. 4: the solution where only $m_j=1,\ -1$ components are coupled ($\delta_2=\eta_2=\delta_0=0$).

Sol. 5: the solution where all the m_j components ($m_j=2,1,0,-1,-2$) are coupled (the most general solution).

In § 4, we have treated the simple solutions (Sol. 1 and Sol. 2) and found their properties. The next step is to compare them with Sol. 3 which results from the coupling of Sol. 1 and Sol. 2 by the ϕ-dependence in $D_\lambda^2(\boldsymbol{k})$, which is limited to $\sin 2\phi$ and $\cos 2\phi$. Putting $\delta_1=\eta_1=0$ in Eq. (16), we have a somewhat simpler gap equation, where the squared energy gap is

$$D_\lambda^2(\boldsymbol{k})=\frac{1}{8\pi}\Big[3(\delta_2^2(k)+\eta_2^2(k))\sin^2\theta+\frac{1}{2}\delta_0^2(k)\,(1+3\cos^2\theta)$$
$$+\sqrt{6}\delta_0(k)\,(\eta_2(k)\sin 2\phi-\delta_2(k)\cos 2\phi)\sin^2\theta\Big]. \qquad (21)$$

Calculations in this section have been performed only for G3RS ${}^3O-1$ potential in order to avoid too long computing time. These gap functions are shown in Fig. 8(a) for $E_F=100$ MeV and $m^*=1$. Calculations are done by the iterative method. Their values at $k=k_F$ are as follows:

$\delta_2(k_F)=1.20$ MeV,

$\eta_2(k_F)=1.08$ MeV,

$\delta_0(k_F)=1.33$ MeV.

For $E_F=75$ MeV and $m^*=0.8$, we have obtained $\delta_2(k_F)=0.24$ MeV, $\eta_2(k_F)=0.22$ MeV, $\delta_0(k_F)=0.27$ MeV.

Similarly, as for Sol. 4, putting $\delta_2=\eta_2=\delta_0=0$ in Eq. (16), we obtain the gap equation for $m_j=\pm 1$ coupling. The resulting energy gap components $\delta_1(k)$, $\eta_1(k)$ are similar to those of the $m_j=\pm 2$ coupling (Sol. 1; $\delta_2(k)=\eta_2(k)$), although in this case the ϕ-dependence of the energy gap makes

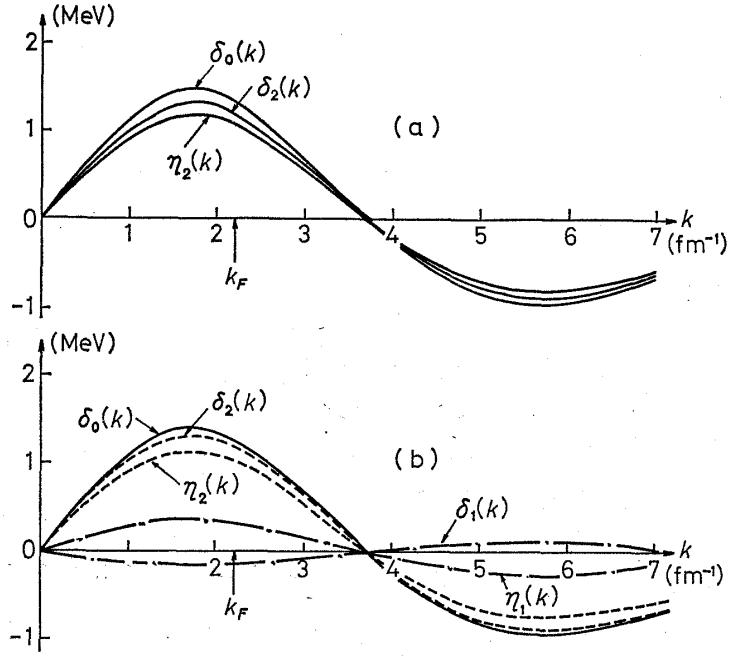

Fig. 8. Components $\delta_2(k)$, $\eta_2(k)$ etc. contained in the energy gap $D_\lambda(\boldsymbol{k})$ calculated from G3RS ${}^3O-1$ for $E_F=100$ MeV and $m^*=1$. Fig. 8(a) for Sol. 3 ($m_j=0,\pm 2$ components are coupled) and Fig. 8(b) for Sol. 5 (all the m_j components ($m_j=2,1,0,-1,-2$) are coupled).

$\delta_1(k)$ slightly different from $\eta_1(k)$. The values of $\delta_1(k)$ and $\eta_1(k)$ for G3RS ${}^3O$ -1 potential at $k=k_F$ are as follows:

$$\delta_1(k_F)=1.296\ \text{MeV}, \qquad \eta_1(k_F)=1.299\ \text{MeV}$$

for $m^*=1$ and $E_F=100$ MeV.

Our main concern is to solve the most generalized equation (16) with all the m_j components and to find the properties of Sol. 5. Equation (16) can be solved by the iterative method, based on the results already obtained. The starting values that make iteration converge are found for respective components ($\delta_2(k), \eta_2(k), \delta_0(k), \delta_1(k)$ and $\eta_1(k)$) of the energy gap $D_\lambda^2(\boldsymbol{k})$. The values of gap components at $k=k_F$ are

$$\delta_2(k_F)=1.21\ \text{MeV}, \quad \eta_2(k_F)=1.04\ \text{MeV}, \quad \delta_1(k_F)=-0.12\ \text{MeV},$$
$$\eta_1(k_F)=0.34\ \text{MeV} \quad \text{and} \quad \delta_0(k_F)=1.27\ \text{MeV}$$

for $m^*=1$ and $E_F=100$ MeV, where k-dependences are shown in Fig. 8(b).

The above values show that the mixing ratio of the $m_j=\pm 1$ components are quite small, and the essential feature of the general solution is the same as that of Sol. 3.

The m^* dependence and the E_F dependence of these solutions (Sol. 3, Sol. 4 and Sol. 5) are qualitatively similar to those of the solutions (Sol. 1 and Sol. 2) that are already mentioned in § 4.

§ 6. Discussion on calculated results

In this section we discuss several consequences based on somewhat detailed properties of the solutions of the ${}^3P_2$ gap equation obtained in §§ 4 and 5. Here we pay attention to the following two points: One is what solution is considered to give the ground state of the system, and the other is what shape of deformation of the Fermi sphere can be expected for the ground state. Finally comments on the ${}^1D_2$ pairing are made.

6-1 *Total energy shift and critical temperature*

The total energy shift is estimated by use of Eq. (11):

$$\Delta E \simeq -N_F \int d\hat{k} D_\lambda^2(k_F, \hat{k})/8\pi,$$

where $N_F=3N/4E_F$ is the level density at k_F for the total neutron number N. By angular integration, all the cross terms are dropped, and the explicit form for each solution is expressed as

Sol. 1 ($m_j=\pm 2$):
$$\Delta E_{m_j=\pm 2} = -N_F/8\pi \cdot |\Delta_2(k_F)|^2$$
$$= -N_F/8\pi \cdot (\delta_2^2(k_F)+\eta_2^2(k_F)),$$

Sol. 2 ($m_j=0$):
$$\Delta E_{m_j=0} = -N_F/16\pi \cdot \Delta_0^2(k_F) = -N_F/16\pi \cdot \delta_0^2(k_F),$$

$$\text{Sol. 3 } (m_j=0,\pm2): \quad \Delta E_{m_j=0,\pm2}=-N_F/8\pi\cdot[\delta_2^2(k_F)+\eta_2^2(k_F)+\tfrac{1}{2}\delta_0^2(k_F)],$$

$$\text{Sol. 4 } (m_j=\pm1): \quad \Delta E_{m_j=\pm1}=-N_F/8\pi\cdot[\delta_1^2(k_F)+\eta_1^2(k_F)],$$

$$\text{Sol. 5 } (m_j=\pm2,\pm1,0): \quad \Delta E_{m_j=\pm2,\pm1,0}=-N_F/8\pi \times[\delta_2^2(k_F)+\eta_2^2(k_F)+\delta_1^2(k_F)+\eta_1^2(k_F)+\tfrac{1}{2}\delta_0^2(k_F)]. \tag{22}$$

The numerical results of ΔE calculated from G3RS ${}^3O-1$ potential for $E_F=100$ MeV and $m^*=1$ are:

$$\begin{aligned}
&\text{(A)} \quad \Delta E_{m_j=\pm2}=-(N_F/8\pi)\,3.37\ \text{MeV}\to3.3669\,,\\
&\qquad\ \ \Delta E_{m_j=\pm1}=-(N_F/8\pi)\,3.37\ \text{MeV}\to3.3770\,,\\
&\text{(B)} \quad \Delta E_{m_j=0}=-(N_F/8\pi)\,3.48\ \text{MeV}\to3.4803\,,\\
&\qquad\ \ \Delta E_{m_j=0,\pm2}=-(N_F/8\pi)\,3.48\ \text{MeV}\to3.4804\,,\\
&\qquad\ \ \Delta E_{m_j=\pm2,\pm1,0}=-(N_F/8\pi)\,3.48\ \text{MeV}\to3.4811\,.
\end{aligned} \tag{23}$$

Roughly speaking, all the solutions are almost degenerate. However, a small but significant difference can be seen between class (A) and class (B); class (B) has a lower ground state energy. The ground state probably lies in class (B). The same tendency is found for $E_F=75$ MeV and $m^*=0.8$. In order to find whether three solutions in class (B) are precisely degenerate or not, we quote two more figures within the accuracy of iterative procedure on the right of (23). Sol. 5 gives the lowest energy but this statement is a very delicate one, since the splittings are too small. Although the energy comparison is delicate, we have a reasoning that Sol. 5 is appropriate to represent the ground state, because this solution is the most general self-consistent solution of the gap equation.

Why do these solutions show such close energy shifts? The reason concerning the Sols. 1 and 2 has been mentioned in § 4; $\Delta_0(k_F)\simeq\sqrt{2}\Delta_2(k_F)$ but the factor $\sqrt{2}$ is cancelled by the number of components as in (22). There may be another explanation in connection with the critical temperature T_c. If we suppose that all the components $\Delta_{\lambda m_j}(k)$ in $D_\lambda(\boldsymbol{k})$ disappear simultaneously at T_c, the equation to determine T_c becomes

$$1=-\left(\frac{1}{\pi}\right)\int_0^\infty dk'k'^2\langle k'|V_\lambda|k'\rangle\frac{\tanh(|\tilde{\varepsilon}_{k'}|\beta_c/2)}{|\tilde{\varepsilon}_{k'}|}$$

for a nonlocal-separable potential, where $\beta_c=\kappa T_c$. For the axially symmetric cases (Sol. 1 and Sol. 2), we have the approximate relations

$$\kappa T_c\simeq0.57\times\begin{cases}\Delta_2(k_F)/\Gamma_2 & \text{for } m_j=\pm2\,,\\ \Delta_0(k_F)/\sqrt{2}\Gamma_0 & \text{for } m_j=0\,,\end{cases}$$

where $\ln\Gamma_2=1.20$ and $\ln\Gamma_0=1.22$.[5] Thus T_c related closely to the energy gap is independent of the types of solutions, in the first approximation. Therefore

we can expect almost the same energy shifts among five possible solutions.

6-2 *Deformation of the Fermi sphere*

Anisotropy is characteristic of the ${}^3P_2$-energy gap, contrary to the isotropic ${}^1S_0$ energy gap.

As already mentioned in the preceding sections, $m_J=\pm 2$ coupling (Sol. 1) and $m_J=0$ coupling (Sol. 2) are axially symmetric and have only the θ-dependence. The former is oblate, having nodes at $\theta=0,\ \pi$. The latter is prolate, but is nodeless with the maximum energy gap at $\theta=0,\ \pi$ and the minimum one at $\theta=\pi/2$. The angle dependence is shown in Fig. 9.

Sol. 3 ($m_J=0, \pm 2$), Sol. 4 ($m_J=\pm 1$) and Sol. 5 ($m_J=0, \pm 1, \pm 2$) are not axially symmetric. The angular dependence of these solutions depends not only on θ but also on ϕ and is much complicated. As is shown in Fig. 9, the θ-dependences of Sol. 3 and Sol. 5 are smoother than those of other solutions (Sol. 1, Sol. 2 and Sol. 4). This is because of the fact that as far as the θ-dependence is concerned, Sol. 3 is the superposition of Sol. 1 with Sol. 2, and Sol. 5 is the superposition of Sol. 1 and Sol. 2 with Sol. 4. As for the ϕ-dependence, Sol. 5 behaves like Sol. 3 because of the small mixture of the $m_J=\pm 1$ components. Solution 4 has nodes at $\theta=\pi/2,\ \phi=\pi/4$ and $\theta=\pi/2,\ \phi=3\pi/4$, but Sol. 3 and Sol. 5 are nodeless.

As is already mentioned in § 6-1, the ground state of the system is considered to be Sol. 5, so that the Fermi sphere of the ground state deforms in axially asymmetric manner but there is no point on the Fermi surface where the energy gap vanishes. The deformation of the Fermi sphere of the ground state is soft in the θ-direction and rather hard in the ϕ-direction.

The nodeless gap leads to the specific heat of the usual type with the factor $\exp[-\bar{D}_\lambda(k_F)/\kappa T]$ below $T<T_c$, where $\bar{D}_\lambda(k_F)$ is some angular average of $D_\lambda(k_F, \hat{k})$. Also, if we calculate the moment of inertia of the neutron ${}^3P_2$ superfluid by a straightforward application of the cranking model,[14] the nodeless gap leads to a value extremely smaller than the rigid one by $\sim 10^{-19}$.[15] Therefore, a low rotational excitation mode of this fluid is expected to be of the vortex type.[16] Nevertheless we have to pay attention to the existence of normal neutron fluid at the densities, probably $\rho \gtrsim 6\times 10^{14}$g cm^{-3} and $\rho \simeq 1\sim 2\times 10^{14}$g cm^{-3}, where the cranking model gives the rigid-body value to the moment of inertia.[6]

The remarkable ϕ-dependence of the energy gap may be important because after angular momentum projection the ϕ-dependence in the intrinsic state produces the rotational excitation accompanying a nonzero component of the total angular momentum along the z-axis of the body-fixed frame where we have made calculations. The above arguments are valid for pure neutron matter. In the actual situation in neutron stars, the neutron matter is contained in the crust stretched slightly by the centrifugal forces. Because the total energy shifts of five solutions are very similar, the environment of neutron matter with anisotro-

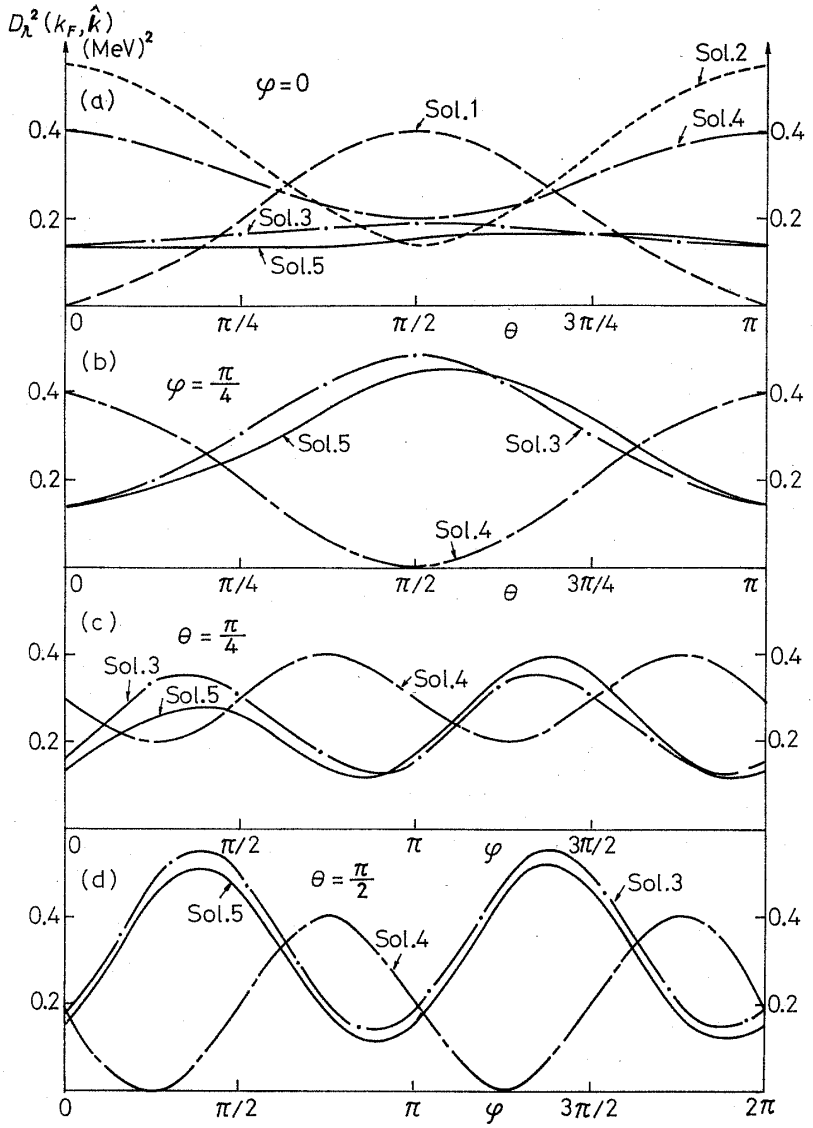

Fig. 9. Angle dependence of various solutions ($D_\lambda^2(k_F,\hat{k})$) calculated from G3RS $^3O-1$ for $E_F=100$ MeV and $m^*=1$: (a) the θ-dependence at $\phi=0$, (b) the θ-dependence at $\phi=\pi/4$, (c) the ϕ-dependence at $\theta=\pi/4$ and (d) the ϕ-dependence at $\theta=\pi/2$.
----: Sol. 1 ($m_j=\pm2$), ·····: Sol. 2 ($m_j=0$), —·—: Sol. 3 ($m_j=0,\pm2$),
———: Sol. 4 ($m_j=\pm1$), ——: Sol. 5 ($m_j=0,\pm1,\pm2$).

pic energy gap may give rise to the occurence of a particular shape of the Fermi surface not necessarily lowest in pure neutron matter.

6-3 *On the* $^1D_2$ *pairing*

The $^1D_2$ pairing interaction is appreciably attractive in the energy region, $E_{N-N}^{(\mathrm{Lab})}\simeq200\sim600$ MeV ($E_F\cong50\sim150$ MeV), although less attractive than that of the $^3P_2$ pair state as shown in Fig. 2. There is a problem whether the coexistence of two types of gap is possible or not. We have found that the energy

gap due to the $^1D_2$ pairing does not take place, by use of OPEG $^1E-1$ potential[12] in solving the gap equation Eq. (4·6) in I restricted to $m_l=0$ only. If we extend the argument concerning the critical temperature in § 6-1, we can say that the $^1D_2$ gap does not exist even for general solutions. Therefore, at high densities only the $^3P_2$ superfluidity prevails.

§ 7. Concluding remarks

The existence of the neutron superfluidity of the $^3P_2$ pairing in the high density region of neutron star matter has been confirmed by solving the general coupled integral equation for the energy gap with several semiphenomenological potentials. In the course of calculation, we have paid attention to short-range forces and the effective mass inferred from the single particle potential obtained by applying the nuclear matter theory to neutron star matter.[13]

The magnitude of the $^3P_2$ gap is very sensitive to both the effective mass and repulsive core in the $^3P_2$-effective potential: It is of the order of MeV at the densities $\rho\simeq 2\times10^{14}\sim1.5\times10^{15}$g cm^{-3} for $m^*\simeq1$, but decreases by about one order for $m^*\simeq0.8$, a realistic value for $\rho=2\sim4\times10^{14}$g cm^{-3}, and vanishes for $m^*\lesssim0.7$, a probable value for $\rho\gtrsim8\times10^{14}$g cm^{-3}. In any case there exists the $^3P_2$-superfluid state at least in the density region, $\rho\simeq(2\sim5)\times10^{14}$g cm^{-3}. A potential without repulsive core *in the* $^3P_2$ *state* allows a somewhat wider region for existence of the $^3P_2$-super state. Even in this case it seems unprobable that this region extends beyond $\rho\sim1\times10^{15}$g cm^{-3}.

We have found the most general solution of the $^3P_2$ gap equation as well as all the possible solutions. A kind of self-consistency implied in this gap equation, besides the demand by the energy consideration, forces us to regard the most general solution (all the m_j components are mixed) as a state to be adopted in the ground state of pure neutron matter. Even though the environment surrounding the neutron matter may lead to complicated situation, we can expect that the $^3P_2$ gap is nodeless and has a rather strong axial asymmetry.

At the end, we want to discuss about the mass of a neutron star, in connection with the argument concerning the superfluidity in the interior of the Vela pulsar given by Baym, Pethick, Pines and Ruderman:[2] The remarkably long relaxation time of the order of years after the discontinuous speed up denotes an indication of the superfluidity of major parts of both the neutron and proton liquids. The proton density is so low that protons are considered to be in the $^1S_0$-superfluid state. Let us take the region of neutron superfluidity as $\rho\lesssim1\times10^{14}$g cm^{-3} for the $^1S_0$ pairing and $\rho\simeq(2\sim5)\times10^{14}$g cm^{-3} for the $^3P_2$ pairing. For a neutron star with small mass such as $M/M_\odot\simeq0.16$, normal fluid occupies a large portion extending from radial distance 2 km to 6 km, on the basis of the recent results of neutron star models.[13] On the other hand, for a neutron star with large mass such as $M/M_\odot>1$, superfluid exists only at a very thin region near

the surface. Therefore, the mass of the Vela pulsar seems to be of the order of $(1/2\sim1/3)M_{\odot}$. This conjecture, of course, is too simple but will serve as an indication to the pulsar mass.[17]

In this connection, the region $\rho\simeq(1\sim2)\times10^{14}$g cm^{-3} should be more carefully investigated, since both the $^1S_0$ and $^3P_2$ gaps vanish or are vanishingly small. Therefore, the effect of the $^3F_2$ coupling cannot be neglected in treating this region.

Acknowledgements

The authors would like to thank Professor S. Nagata, Professor T. Tsuneto and members of the laboratory of Professor C. Hayashi for their valuable discussions. One of the authors (T.T.) is grateful to Professor Y. Katayama for continuous encouragement. Numerical calculations were performed using the FACOM 230-60 in the computer center of Kyoto University.

References

1) R. Tamagaki, Prog. Theor. Phys. **44** (1970), 905.
2) G. Baym, C. Pethick, D. Pines and M. Ruderman, Nature **224** (1969), 872.
3) Prog. Theor. Phys. Suppl. No. 3 (1956); No. 39 (1967); No. 42 (1968).
4) M. Hoffberg, A. E. Glassgold, R. W. Richardson and M. Ruderman, Phys. Rev. Letters **24** (1970), 775.
5) P. W. Anderson and P. Morel, Phys. Rev. **123** (1961), 1911.
6) R. D. Amado and K. A. Brueckner, Phys Rev. **115** (1959), 778.
R. M. Rockmore, Phys. Rev. **118** (1960), 1645.
7) K. A. Brueckner, T. Soda, P. W. Anderson and P. Morel, Phys. Rev. **118** (1960), 1442.
8) L. N. Cooper, R. L. Mills and A. M. Sessler, Phys. Rev. **114** (1959), 1377.
9) T. Marumori, T. Murota, S. Takagi, H. Tanaka and M. Yasuno, Prog. Theor. Phys. **25** (1961), 1035.
10) T. Ishihara, R. Tamagaki, H. Tanaka and M. Yasuno, Prog. Theor. Phys. **30** (1963), 601.
11) T. R. Mongan, Phys. Rev. **178** (1969), 1579.
12) R. Tamagaki, Prog. Theor. Phys. **39** (1968), 91.
13) S. Ikeuchi, S. Nagata, T. Mizutani and K. Nakazawa, Prog. Theor. Phys. **46** (1971), 95.
14) D. R. Inglis, Phys. Rev. **96** (1954), 1059; **103** (1956), 1786.
15) Y. Shono, Report at the Symposium on "Magnetic Properties of Neutron Gas", held Feb. 25~26, 1970, Mito, Japan.
16) V. L. Ginzburg and D. A. Kirzhnitz, J. Exptl. Theor. Phys. (USSR) **47** (1964), 2006.
G. Baym, C. Pethick and D. Pines, Nature **224** (1969), 673.
17) P. Sutherland, G. Baym, C. Pethick and D. Pines, Nature **225** (1970), 353.